Determination of the structure of the organized phase of the block copolymer PEO-PPO-PEO in aqueous solutions under flow by small-angle neutron scattering

Christelle Perreur, Jean-Pierre Habas, Jeanne François, and Jean Peyrelasse*
Laboratoire de Physico-Chimie des Polymères UMR 5067, Université de Pau et des Pays de l'Adour Avenue de l'Université, 64000 PAU, France

Alain Lapp
Laboratoire Léon Brillouin, CEA Saclay, 91191 GIF-sur-YVETTE Cedex, France
(Received 4 April 2001; revised manuscript received 10 September 2001; published 3 April 2002)

The organization of Tetronic 908® (T908), a star copolymer of poly(ethylene oxide) (PEO) and poly(propylene oxide) (PPO) blocks, has been examined. Above critical conditions of temperature and concentration, the micelles formed by the aggregation of PPO units self-organize into particular structures. While small-angle neutron scattering (SANS) characterizations performed with static conditions demonstrate the organization of the medium, the experimental results do not allow us to make a distinction between simple cubic and body-centered-cubic structures. However, SANS measurements realized under shear produce characteristic diffraction diagrams. In this paper, an accurate methodology is proposed to identify, without ambiguity, the exact nature of the organized phase. Applied to our system, indexing of the diffraction pattern spots reveals that the organization of T908 is of bcc type oriented with the [111] direction parallel to the direction of flow, but the crystals can present any orientation about this direction. The lattice size has been estimated and compared to previous published results.

DOI: 10.1103/PhysRevE.65.041802 PACS number(s): 61.25.Hq, 61.12.Ld, 61.12.Ex

I. INTRODUCTION

Many studies have been performed on copolymer blocks composed of poly(oxyethylene) (PEO) and poly(oxypropylene) (PPO) in aqueous solution. The system most often studied is PEO-PPO-PEO, but it is also possible to find results in the literature regarding the study of copolymer solutions of the type PPO-PEO-PPO [1,2] in water or PEO-PPO-PEO in oil-water mixtures [3,4]. At low temperatures, these copolymers are water soluble. However, when the temperature is increased, the solubility of PPO is reduced and the polymers aggregate to form micelles. Most of copolymers studied in the literature are linear (Pluronic®). However, in a recent paper, we characterized the structure and the rheological properties of aqueous solutions of Tetronic 908®. This compound is a four-branched star copolymer comprised of PEO and PPO blocks fixed on an aliphatic diamine.

Since the micelle size is small (up to 100 Å), the most efficient techniques for studying the structure of these solutions are small-angle x-ray scattering (SAXS) or small-angle neutron scattering (SANS). In a neutron scattering experiment, the diffused intensity (I) is measured according to the module of the wave vector (q) and is defined by

$$I(q)=N\Delta\rho^2P(q)S(q),$$

where $q=(4\pi/\lambda)\sin(\theta/2)$. θ is the scattering angle, λ the wavelength, N is the number density of micelles, $\Delta\rho^2$ the contrast factor, $P(q)$ the form factor, and $S(q)$ the structure factor.

The expression of $S(q)$ depends on the interaction potential between the micelles (hard spheres, hard spheres plus step [5], adhesive spheres [6] and so on). For diluted solutions, in which the micellar correlations are negligible, $S(q)=1$. The form factor depends on the model that has been chosen to describe the micelles. For instance, Mortensen and co-workers [1,2,7,8] proposed that the micelles consist of a core of PPO with a radius R_c containing a small percentage of PEO. The shell made up of both PEO and water was not included in the calculations. Liu *et al.* [6] proposed a two-shell model made up of PPO in the core and PEO and water in the corona. This model supposed that all the polymer is micellized. Goldminst *et al.* [9,10] and Yang *et al.* [11] both proposed a rather similar two-layer model, the main difference being the possibility of presence of water both in the core and in the shell. Unfortunately, these different models cannot explain our results with T908 solutions. For this reason, we have proposed a three-layer model, showing an equilibrium state between unimers and micelles. This model perfectly fits the experimental curves $I(q)$ [12,13].

In many cases, when aqueous solutions of PEO-PPO-PEO are heated, they exhibit a transition resembling that obtained with sol gel. This is due to the spatial organization of micelles and is visible in the evolution of the viscosity that strongly increases [12–17]. The structure of the organized phases depends not only on temperature, concentration, and solvent, but also on the relative amounts of ethylene oxide and propylene oxide present in the polymer chain.

Several studies using SANS or SAXS techniques, have been published on the ability of the organized structures to orientate under shear. There remains, however, considerable confusion concerning the interpretation of these experiments. Plutonic F127, $EO_{99}PO_{69}EO_{99}$, can be considered a good

*Author to whom correspondence should be addressed. Email address: jean.peyrelasse@univ-pau.fr

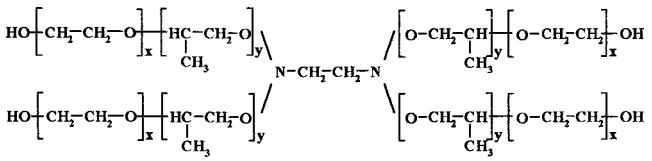

FIG. 1. Chemical structure of Tetronic 908®.

example of this problem. Although it has been studied by several authors, contradictory information abounds in the literature. According to Lenaerts *et al.* [18], the micelles could not self-organize. Wu *et al.* [19], however, proposed the formation of a face-centered-cubic lattice (fcc). The paper of Prud'homme, Wu, and Schneider [20] excluded the possibility of this latter structure. However, their results did not allow the distinction between a simple cubic (sc) lattice or a centered cubic (bcc) organization. The conclusions of their study are in agreement with Mortensen's work [8]. Eiser *et al.* [21] have studied Pluronic® F108, $EO_{127}PO_{48}EO_{127}$, which has a structure close to that of F127. The authors concluded that their SAXS results were due to a fcc type. Although the bcc-fcc transitions have not previously been demonstrated, their existence could explain this difference in interpretation. Different types of transition have been already described for other systems. For example, Mortensen [8] showed the complexity of the phase diagram for P85, $EO_{25}PO_{40}EO_{25}$, in relation to the temperature and the polymer concentration; the organized phases can be bcc, lamellar or hexagonal. Studies of Pluronic® 109, $EO_{17}PO_{60}EO_{17}$, solubilized in a *p*-xylene-water mixture, highlighted the existence of a lamellar structure [22] whilst Zhou, Su, and Chu [23] demonstrated that a transition fcc-hexagonal structure existed. King *et al.* [24], using the same polymer in aqueous solution have demonstrated the formation of solid rodlike micelles. Holmqvist, Alexandridis, and Lindman [25] observed the presence of cubic, hexagonal and lamellar structures for Pluronic® 127 in solution in a *p*-xylene-water mixture. Alexandridis, Zhou, and Khan [26] showed, with the study of a series of copolymers (L62, L64, P105), the ability to get, according to temperature and concentration of polymer, cubic, hexagonal or lamellar phases. It is worth noting that other diblock copolymers such as poly(oxyethylene)-poly(oxybutylene) [27–29] or poly(ethylene)-poly(dimethylsiloxane) [30] exhibit a similar behavior as previously detailed for PEO-PPO systems. To sum, a fuller understanding of these systems is required to explain the discrepancies found between different studies.

The goal of this article is to show that it is possible to determine, without ambiguity, the structure of the organized phases and to quantitatively determine the lattice parameters by the use of the neutron scattering coupled with a flow technique.

II. EXPERIMENTAL SECTION

A. Samples

Tetronic® from BASF consists of poly(ethylene oxide), PEO, and poly(propylene oxide), PPO blocks joined to an aliphatic diamine as shown in Fig. 1. In this paper, we studied the properties of T908 ($M = 25\,000$ g mol^{-1}). The mean numbers of EO and PO units per branch are respectively $x = 114$ and $y = 21$ and it was used without further purification. Aqueous solutions were prepared at low temperature ($T \approx 3$ °C) under stirring, using bidistilled water for all rheological experiments and deuterated water, D_2O, for the small-angle neutron scattering studies. All solutions are expressed by weight percentages.

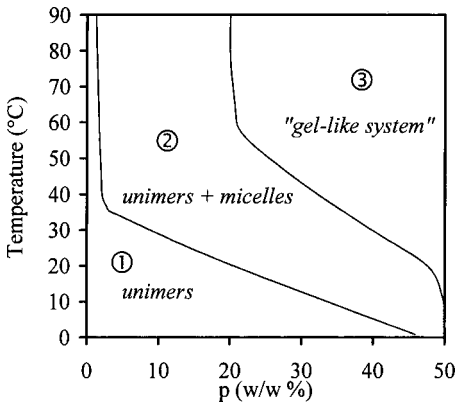

FIG. 2. Phase diagram of aqueous solutions of Tetronic 908®.

B. Small-angle neutron scattering

SANS experiments were performed at the laboratoire Léon Brillouin, CEA de Saclay (France) on the PAXY spectrometer. A wavelength of 8 or 6 Å (with a resolution of 10%) was selected, and an effective distance between the sample and the detector was 3.2 m. This allowed a momentum transfer range of 0.1 to 1.2 nm^{-1}. Data correction allowed for sample transmission and detector efficiency. The efficiency of the detector was taken into account with the scattering of H_2O. Absolute intensities were obtained by reference to the attenuated direct beam, and the scattering of pure solvent was subtracted. Finally, intensities were corrected for a small solute-incoherent contribution. When the scattering patterns of the samples were isotropic, the one-dimensional data set was generated by circular integration of the corresponding two-dimensional (2D) patterns. For static measurements, quartz cells were used with 2 or 1 mm path length. For the measurements under shear, we used a thermostated Couette cell with a rotation speed of 0–800 rpm. The walls of the cell were made of quartz and the external cylinder was mobile ($\Phi = 47.24$ mm), whilst the internal cylinder ($\Phi = 43.43$ mm) was fixed. The height of the inner cylinder was 55 mm. With respect to the cell, the shear rate varied between 0 and 955 s^{-1}.

III. RESULTS

A. Phase diagram

In a previous paper [12], from viscosimetric measurements, we determined the phase diagram of the aqueous solution of T908 (Fig. 2). This study demonstrated that in zone 1, the solution contains only unimers. In zone 2, there is an equilibrium between unimers and micelles, which moves to-

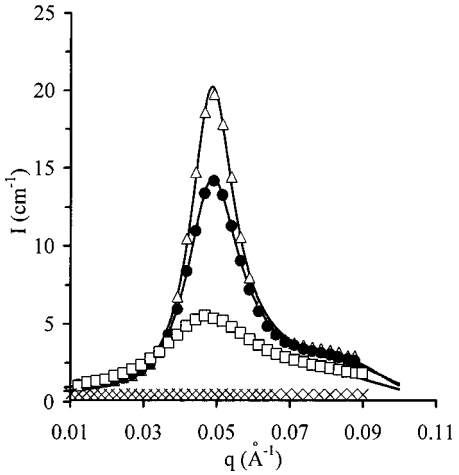

FIG. 3. Effect of temperature on scattered intensity of a 30% solution: ×, 5 °C; □, 20 °C; ●, 30 °C; △, 37 °C.

wards micelles when the temperature increases. The limit between zone 1 and zone 2 makes it possible to define, for each concentration, the critical micelle temperature. These results were also confirmed by other techniques (light scattering, fluorimetry, SANS). The transition between zones 2 and 3 is characterized by the divergence of the viscosity above the temperature T_d, which depends on concentration. Measurements by mechanical spectroscopy clearly showed that this phenomenon is not a sol-gel transition. Indeed, beyond the temperature T_d, the solutions, when exposed to the lowest frequencies, exhibited a rheological behavior similar to that of entangled polymers [12]. When the temperature was increased, the crossover point moved towards the low frequencies, i.e., long relaxation times.

B. Static SANS studies

SANS measurements were taken in the different zones of the phase diagram. In zone 1, which corresponds to unimers in solution, the $I(q)$ spectra are flat. In contrast, in zone 2 of the diagram, $I(q)$ reveals a peak whose amplitude increases with temperature (Fig. 3). This peak corresponds to the formation of micelles and its rise in intensity is the result of an increase in the volume fraction of micelles. The peaks can be fitted using a hard-sphere model. With the model that we developed [12,13], several parameters can be determined such as the radius of the micelles, their volume fraction, the fraction of unimers in equilibrium with the micelles, and the fraction of water contained within the micelles. Figure 3 shows a very good match between the model and experimental results.

In zone 3 of the phase diagram, Bragg peaks are revealed thus showing a transition to an organized phase. The 2D pattern is isotropic, this is equivalent to a crystal powder diffraction diagram and clearly indicates that the crystals exhibit all possible orientations in space (Fig. 4).

The amplitude of the scattering vector q is defined by $q=(4\pi/\lambda)\sin(\theta/2)$, where θ is the scattering angle and λ the wavelength. Using the Bragg relation $2d\sin(\theta/2)=\lambda$, one can see that the values of q at the successive maxima are

FIG. 4. 2D diffraction diagram of a 40% solution at $T=70$ °C.

given by $q_i=2\pi/d_i$. Our experimental results give $q_2/q_1=d_1/d_2\approx\sqrt{2}$, and $q_3/q_1=d_1/d_3\approx\sqrt{3}$. This shows that the structure is cubic. It is not possible to determine if it is a simple or centered cubic lattice, but we can exclude the formation of a face-centered-cubic lattice. To investigate the exact nature of the network, concentrated solutions of 30% and 40% were studied using SANS under flow by varying the temperature and the shear rate.

C. SANS studies under flow

In zone 2 of the diagram, there are no observable differences between the results from samples under static or shear conditions. But in zone 3, where the micelles are organized and form a cubic lattice, the differences are fundamental. The 2D diffraction figures were found to be isotropic for static

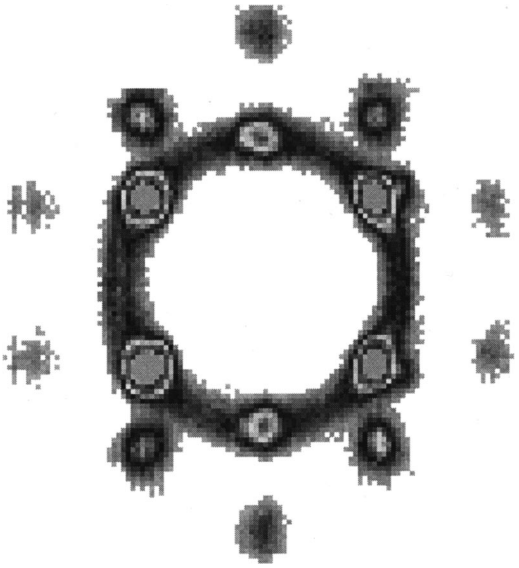

FIG. 5. 2D diffraction pattern of a 30% solution under shear ($\dot{\gamma}=371\ s^{-1}$) at $T=47$ °C.

samples but anisotropic for those under shear. Figure 5 presents results for a sample containing a 30% polymer with a wavelength of 6 Å and a shearing rate of 371 s^{-1} is characteristic (an image editing program was used to eliminate the background noise).

The cubic polycrystals, which were dispersed in a random way at rest, oriented themselves in the shearing direction. However, the isotropic part of the diffraction spectra did not completely disappear, indicating the presence of crystals with orientations distributed at random. This could be explained by wall-slips phenomenon in the Couette cell. On changing the shear rate, the maximum orientation seemed to be obtained very quickly for shear rate of about 200 s^{-1}. No changes were detected in the diffraction pattern, even for high shear rates up to 950 s^{-1}. This shows that for the system studied, the shear does not induce nonequilibrium or transitory structures. It can also be noted that once created, the orientation remains for a long period of time; some orientated samples exhibited the same pattern after a rest of several hours. This is not surprising considering the great viscosity of the medium.

IV. DISCUSSION

A. Analysis of the figures of diffraction obtained under flow

1. Nature of the network

Figure 5 shows that diffraction spots are distributed in some vertical and equidistant layers, as well as in concentric circles: it resembles an x-ray diffraction diagram obtained by the rotating crystal method. Below we describe some fundamental results of this method.

A monocrystal with an unspecified position related to an incidental beam does not generally give any diffracted rays, since the Bragg relation is not satisfied. In order to obtain a complete diffraction figure, the crystal must be turned about a direction perpendicular to the incidental beam. During the rotation, each reticular plane having an angle to the incident beam that satisfies the Bragg relation, makes possible a reflection (this condition occurs whenever a reciprocal lattice point lies exactly on the Ewald sphere). The diffraction pattern remains relatively simple to analyze if the axis of rotation remains parallel to a particular row $[uvw]$ of the crystal. It is well known that the diffracted beams are located in the equatorial plane (the plane containing the incidental beam and perpendicular to the crystal row $[uvw]$ and on cones of revolution, around the axis of rotation. All this results in a spot diagram.

In classical experiments, the incident beam is horizontal and the axis of rotation is vertical. The diffracted rays are recorded into a film that is wrapped around a cylindrical chamber with the same vertical axis as the axis of rotation. The spots are distributed in horizontal layers (intersection of cones with the cylinder). Each spot is the result of a diffraction by a reticular plane $\{hkl\}$. Spots from the layer of order n verify the following equation:

$$ub+vk+wl=n. \tag{1}$$

Moreover, the distances l_i from the ith layers to the equatorial layer is given by

$$l_i=\frac{D\times i}{\sqrt{(L^2/\lambda^2)-i^2}},$$

where D is the radius of the chamber and L the distance between two consecutive nodes on the $[uvw]$ row. If $(L/\lambda)^2$ is much bigger than i^2 and if we only consider the first layers, the latters are equidistant and have a gap Δ given by

$$\Delta=\frac{D\lambda}{L}. \tag{2}$$

Our theory is that the monocrystals, which exhibited all possible orientations in space in a static experiment, now orientate themselves with shearing, in such a way that one direction of the crystals is perpendicular to the incident beam, but about this direction, all orientations are possible. The result obtained will be identical to that using a monocrystal rotated about the same direction.

In the case of SANS, the diffraction pattern is not recorded on a cylinder coaxial to the axis of rotation of the crystal as used with x-ray but on a plane multidetector. However, the scattering angles are very small and the distance between the sample and the detector is great enough to assume that the equations applied with x-ray diffraction remain correct.

The observed layers are vertical and thus the crystals are oriented with a row $[uvw]$ in a horizontal direction perpendicular to the incident beam. The type of crystal (simple cubic or centered) and the particular row $[uvw]$ are still to be determined in order to explain the diffraction pattern.

The different spots are distributed in concentric circles; those that are located on the same circle have the same scattering angle. According to the Bragg relation, this is characteristic of diffraction through identical $\{hkl\}$ planes (same d_{hkl}).

According to the scale factor, the radius of the three circles on the multidetector are respectively 14.9, 21, and 25.7 cm. As the radii are proportional to q, they are inversely proportional to d_{hkl}. We get $r_3/r_1=d_1/d_3=1.72$ and $r_2/r_1=d_1/d_2=1.41$. These ratios are very close to $\sqrt{3}$ and $\sqrt{2}$.

This result confirms again the existence of a sc or bcc structure. The layers are equidistant and thus the approximation $(L/\lambda)^2 \gg i^2$ must be satisfied. The distance between the layers is then given by $\Delta=D\lambda/L$ [Eq. (2)], where D is now the distance sample-detector.

It is possible to determine the nature of the network and the row $[uvw]$ around which the crystals are oriented in a relatively simple way. If r_1 is the radius of the first circle, the scattering angle θ_1 for the spots belonging to this circle is given by $\tan\theta_1=r_1/D$. As the angles are very small, we obtain

$$\sin\frac{\theta_1}{2}=\frac{\lambda}{2d_{hkl}}=\frac{r_1}{2D} \quad \text{and then} \quad \frac{r_1}{\Delta}=\frac{L}{d_{hkl}}.$$

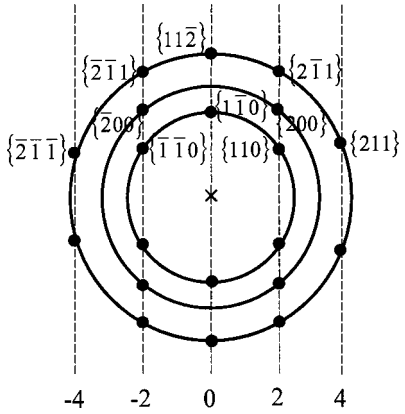

FIG. 6. Theoretical figure of diffraction for a bcc system with the direction [111] in the flow direction: indexation of the spots.

Under experimental conditions, we measure $\Delta = 12.1$ cm, then $r_1/\Delta = 1.23$. If the ''crystals'' are bcc and oriented with the raw [111] in the direction of the flow then:

$$L = \frac{a\sqrt{3}}{2} \Rightarrow \frac{r_1}{\Delta} = \frac{\sqrt{6}}{2} = 1.22.$$

One can notice that the last hypothesis is in perfect agreement with the experimental determination, and this solution is the only one possible.

2. Indexing the spots of diffraction

Since the network is a body-centered-cubic one, the spots located on the first circle are of the type {110}, those of the second circle are of the type {200}, and those of the third circle of the type {211}. No spots were observed on the fourth circle because of the q domain limitation.

The crystals move towards the row [111] in the direction of the flow. The vertical layer, which represents the symmetrical axis of the figure of diffraction, corresponds to $n = 0$. It must, therefore, contain the spots $h+k+l=0$ [Eq. (1)], i.e., {1$\bar{1}$0} and {2$\bar{1}\bar{1}$} or {$\bar{2}$11}. These spots are visible

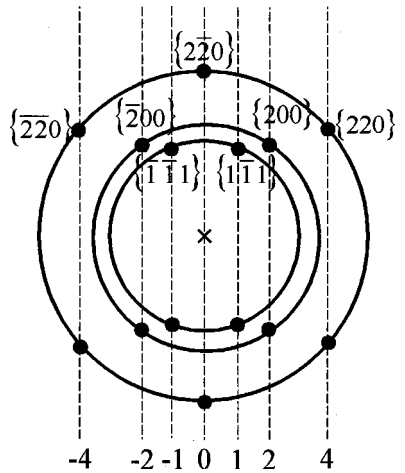

FIG. 7. Theoretical diffraction figure for a fcc system with the direction [111] in the flow direction.

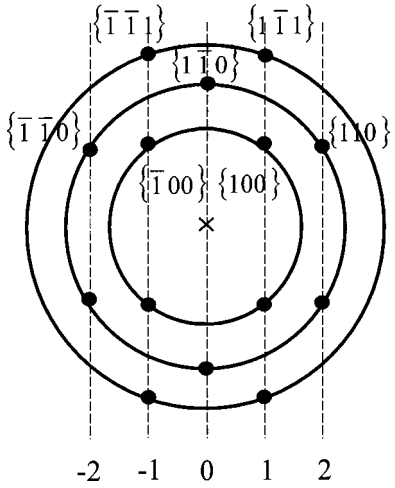

FIG. 8. Theoretical diffraction figure for a sc system with the direction [111] in the flow direction.

on the first and the third circles, which is satisfactory.

On the first layer we must have $h+k+l=2$ (for the bcc lattice the sum of the three indices must be even). The possible spots are {110}, {200} or {2$\bar{1}\bar{1}$}. The first one {110} and {200} are detected. The spot {2$\bar{1}\bar{1}$} on the third circle is not visible, but there is a spot with a low intensity located at the limit of the accessible q domain.

On the second layer $h+k+l=4$. Thus, the first spot must be of type {211}, and is present on the third circle. The above considerations show that it is possible to index all the spots that appear on the pattern. This indexation is shown in Fig. 6. It is then possible to predict the angular positions of different spots. For example, the six spots from the first ring must be separated by four angles of 54.7° and two angles of 70.5°; this is still in perfect agreement with the experimental observations.

Assuming that the hypothesis we have formulated is correct, Figs. 6, 7, and 8 illustrate what should be the theoretical patterns for the bcc, fcc, and sc systems when the crystals orient with the direction [111] in the direction of flow. Let us note that in the cubic lattices, the rows [uvw] are perpendicular to the reticular planes {uvw}. The reticular planes {111}

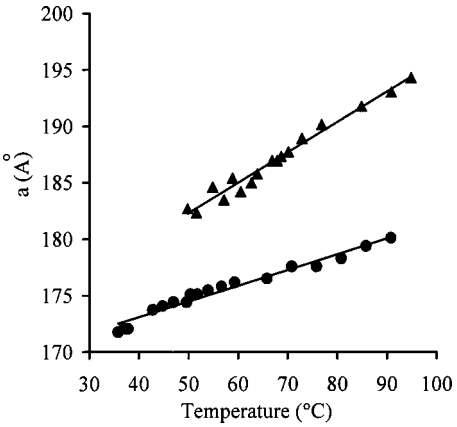

FIG. 9. Evolution of the lattice parameter according temperature for a 30% (▲) and a 40% (●) solutions.

are thus parallel to the incident beam and the reflections {111} do not exist (see on Figs. 7 and 8, the absence of spots on the third layers).

We note that these figures are sufficiently different such that one can, without any ambiguity, determine the structure even if it is only possible to see the first-order diffraction spots.

3. Lattice parameters

The radii r_i of the circles representative of the reflections {110}, {200} or {211} are defined by $r_1=\sqrt{2}\lambda D/a$, $r_2=2\lambda D/a$, $r_3=\sqrt{6}\lambda D/a$. The parameter a of the network can thus be calculated. Its average value is equal to 183 Å.

It is also possible to check these calculations by evaluating the equidistance Δ between the layers. $\Delta=12.1$ cm and the distance between two nodes in the direction [111], which is the diagonal of the cube, is given by $L=D\lambda/\Delta$. We obtain $L=158$ Å and since $a=2L/\sqrt{3}$, we find that $a=183$ Å and this is in perfect agreement with previous determinations.

Knowing L, one can check that the hypothesis $(L/\lambda)^2 \gg i^2$ is validated since $(L/\lambda)^2=693$ and that for the second layer $i^2=4$. In a previous paper [12], we have determined the radius R_m and the volume fraction Φ of micelles as a function of temperature and weight percentage. For instance, for a 30% solution at $T=52\,^{\circ}$C, (zone 3 of the phase diagram), we obtain $R_m=71.5$ Å and $\Phi=0.48$. Since the bcc lattice has two micelles by mesh, it is possible to reestimate the lattice size as in

$$a=\left(2\frac{4\pi R_m^3}{3\Phi}\right)^{1/3}.$$

The calculated value, $a=185$ Å, is in perfect agreement with the previous analysis.

We also performed SANS experiments under static conditions with 40% and 30% weight percentage solutions according to the temperature. Knowing now that the network is bcc in zone 3 of the diagram, it is possible to calculate the lattice parameter by using the q position of the first peak. Figure 9 shows the evolution of the lattice sizes in relation to the temperature. It reveals that the lattice parameter of the network decreases when the polymer concentration increases and that the network becomes slightly dilated with an increase in temperature. The dilatation coefficients are 8.1×10^{-4} and $1.5\times10^{-3}\,^{\circ}\mathrm{C}^{-1}$ for 40% and 30% solutions, respectively.

4. Comparisons with results in the literature

Many authors have explained their diffraction figures by considering the existence of twinned structures. In the case of the diblock polymer solutions of polystyrene/polyisoprene in decane, McConnel, Lin, and Gast [31] show that the bcc crystal is twinned with the twinning plane perpendicular to the {110} planes and the twins are oriented at 35.3° with respect to the shear direction. Similar explanations have been suggested by Hamley *et al.* [27] for aqueous solutions of poly(oxyethylene)-poly(oxybutylene), $E_{210}B_{16}$. In the case of the T908 solutions that we studied, the rules of crystallography allow us to interpret the diffraction pattern without any allusion to twinned structures. Our results are consistent with Hamley's data for $E_{86}B_{10}$ solutions that do not present a twinned structure as of $E_{210}B_{16}$ solutions [28]. After orientation of the sample by a large amplitude shearing at high frequency, these authors determine the diffraction pattern for different angles of rotation around the direction [111]. For some angles of rotation, the obtained figure is poor but by superposition of the different patterns, an exact match with Fig. 6 is obtained. Unlike our system for which the crystals can present all orientations around the principal direction [111], Hamley *et al.* obtained an organization that resembles that of a single crystal. The rotation around [111] brings the observed {110}, {200}, {211}, {220} reflections into the Bragg diffracting conditions.

The previous discussion shows that it is rather difficult to establish universal conclusions about the behavior of ''gels'' of copolymer solutions under flow. According to the system studied (changes in viscosity or elastic modulus) and the experimental conditions used, polycrystals that are orientated randomly at rest, orient themselves under flow. In the case of cubic systems, the axis [111] is often the direction of orientation under flow. Twinned structures or crystals with all orientations around a given direction can be obtained such as has been observed with T908. It is also possible to find examples in which the hypothesis of a more favorable direction allows an interpretation of all the observed spots. However, some spots predicted by the laws of crystallography remain absent. This indicates that all crystals have a common direction but some orientations around this common direction are not present in the sample. This is probably the case of the systems studied by Eiser *et al.* for which the spots $\{1\bar{1}0\}$ are not detected [21,32]. It can be noted that such a phenomenon is often observed for laminated metals.

Mortensen [1] studied solutions of 25R8, $PO_{15}EO_{156}PO_{15}$, for which he obtained a six-spot pattern distributed on a circle, with the observed peaks being separated by four angles of 52° and by two angles of 76°. The author was surprised not to obtain a perfect threefold symmetry and thus described it as resulting from a face-centered-cubic lattice. In this paper, we have seen that the plots due to the reticular planes of type {110} for a bcc lattice must be separated by four angles of 54.7° and by two angles of 70.6°. It is thus very probable that the solution of 25R8 also crystallizes in a bcc system.

IV. CONCLUSION

This paper aimed to demonstrate the exact nature of the organized phase, which appeared in a broad zone of the phase diagram for some copolymers of type PEO-PPO-PEO in aqueous solutions. We have shown the significance of using measurements obtained with small-angle neutron scattering from samples under flow. The results do not make it possible to completely differentiate the type of micellar organization when the solutions are at rest, however, a correct analysis of the diffraction pattern from a sample under flow permits the determination of the nature of the sample network as well as the calculation of lattice parameters. We

have shown that with our experimental conditions, the T908 crystals orient themselves with the direction [111] in the direction of flow, but the crystals can present any orientation about this direction. The classical rules of crystallography allow a rigorous interpretation of the obtained diffraction pattern. The previous analysis also permits a preview of the diffraction patterns obtained even if the polycrystals are oriented in a direction different from [111], and can be generalized to apply to comparable polymer solutions. In a following paper, we will show that polymers whose structure is close to that of the compound studied here, can organize into hexagonal structures.

ACKNOWLEDGMENT

We thank Dr. R. C. Hiorns for helping us to prepare this manuscript.

[1] K. Mortensen, Macromolecules **30**, 503 (1997).
[2] K. Mortensen, W. Brown, and E. Jorgensen, Macromolecules **27**, 5654 (1994).
[3] G. Wu, L. Liu, V. B. Buu, B. Chu, and D. K. Schneider, Physica A **231**, 73 (1996).
[4] B. Chu, G. Wu, and D. K. Schneider, J. Polym. Sci., Part B: Polym. Phys. **32**, 2605 (1994).
[5] E. Caponetti, M. A. Floriano, M. Varisco, and R. Triolo, in *Structure and Dynamics of Strongly Interacting Colloids and Supramolecular Aggregates in Solution*, edited by S. H. Chen, J. S. Huang, and P. Tartaglia (Kluwer Academic, London, 1992), Vol. C 369, p. 535.
[6] Y. C. Liu, S. H. Chen, and J. S. Huang, Phys. Rev. E **54**, 1698 (1996).
[7] K. Mortensen and J. S. Pedersen, Macromolecules **26**, 805 (1993).
[8] K. Mortensen, J. Phys.: Condens. Matter **8**, A103 (1996).
[9] I. Goldminst, F. K. von Gottberg, K. A. Smith, and T. A. Hatton, Langmuir **13**, 3659 (1997).
[10] I. Goldminst, G. Y. YU, C. Booth, K. A. Smith, and T. A. Hatton, Langmuir **15**, 1651 (1999).
[11] L. Yang, P. Alexandridis, D. C. Steytler, M. J. Kositza, and J. F. Holzwarth, Langmuir **16**, 8555 (1999).
[12] C. Perreur, J. P. Habas, A. Lapp, J. Peyrelasse, and J. François, Phys. Rev. E **63**, 31 505 (2001).
[13] C. Perreur, J. P. Habas, A. Lapp, J. François, and J. Peyrelasse, Macromol. Symp. **166**, 127 (2001).
[14] P. Bahadur and K. Pandya, Langmuir **8**, 2666 (1992).
[15] W. Brown, K. Schillén, M. Almgren, S. Hvidt, and P. Bahadur, J. Phys. Chem. **95**, 1850 (1991).
[16] P. D. T. Huibers, L. E. Bromberg, B. H. Robinson, and T. A. Hatton, Macromolecules **32**, 4889 (1999).
[17] G. Wanka, H. Hoffmann, and W. Ulbricht, Colloid Polym. Sci. **268**, 101 (1999).
[18] V. Lenaerts, C. Triqueneaux, M. Quarton, F. Rieg-Falson, and P. Couvreur, Int. J. Pharm. **39**, 121 (1987).
[19] C. Wu, T. Liu, B. Chu, D. K. Schneider, and V. Graziano, Macromolecules **27**, 4574 (1997).
[20] R. K. Prud'homme, G. Wu, and D. K. Schneider, Langmuir **12**, 4651 (1996).
[21] E. Eiser, F. Molino, G. Porte, and X. Pithon, Rheol. Acta **39**, 201 (2000).
[22] O. Glatter, G. Scherf, K. Schillen, and W. Brown, Macromolecules **27**, 6046 (1994).
[23] S. Zhou, J. Su, and B. Chu, J. Polym. Sci., Part B: Polym. Phys. **36**, 889 (1998).
[24] S. M. King, R. K. Heenan, V. M. Cloke, and C. Washington, Macromolecules **30**, 6215 (1997).
[25] P. Holmqvist, P. Alexandridis, and B. Lindman, Macromolecules **30**, 6788 (1997).
[26] P. Alexandridis, D. Zhou, and A. Khan, Langmuir **12**, 2690 (1996).
[27] I. W. Hamley, K. Mortensen, G.-E. Yu, and C. Booth, Macromolecules **31**, 6958 (1998).
[28] I. W. Hamley, J. A. Pople, J. P. A. Fairclough, A. J. Ryan, C. Booth, and Y. W. Yang, Macromolecules **31**, 3906 (1998).
[29] C. Daniel, I. W. Hamley, W. Mingvanish, and C. Boot, Macromolecules **33**, 2163 (2000).
[30] M. E. Vilgid, K. Almdal, K. Mortensen, I. W. Hamley, J. P. A. Fairclough and A. J. Ryan, Macromolecules **31**, 5702 (1998).
[31] G. A. McConnell, M. Y. Lin, and A. P. Gast, Macromolecules **28**, 6754 (1995).
[32] E. Eiser, F. Molino, G. Porte, and O. Diat, Phys. Rev. E **61**, 6759 (2000).